

# Tools for Viscoelastic Damping Treatment Design. Application to an Automotive Floor Panel.

Etienne Balmès<sup>†</sup> and Sylvain Germès<sup>‡</sup>

<sup>†</sup>SDTools, 52 rue Vergniaud, 75013 Paris, France and Ecole Centrale Paris, 92295 Chatenay Malabry

e-mail: balmes@sdtools.com

<sup>‡</sup>PSA Peugeot Citroën, Dpt. of Sciences for Automobiles and Advanced Research, 78943 Vélizy-Villacoublay

e-mail : sylvain.germes@mpsa.com

## Abstract

Passive damping treatments are often considered, in the automotive and other industries, to achieve acceptable vibroacoustic behaviour. This paper presents an on-going effort to provide tools to assess, at the design stage, the validity of possible technical solutions. These tools address material representation, meshing of constrained viscoelastic treatments from shell models, and solvers for direct frequency response and eigenvalue solution of moderately detailed problems. The case of an automotive floor panel is then used to illustrate computations that can be needed in a design phase.

## 1 Introduction

Low frequency (20 - 200 Hz) noise reduction in the passenger compartment has emerged in the past few years as a crucial subject of research in the car industry. This kind of noise is mainly due to the panel vibrations, resulting from the propagation of mechanical inputs (engine, trains) in the car body frame. Nowadays, two main techniques are widely applied in the automotive industry in order to address low frequency noise reduction:

- The first one consists in filtering the mechanical inputs close to the vibratory sources. Engine mounts for instance, aim to limit the energy transfers between the engine and the car body frame.
- The second one is based on passive damping systems, which are generally located on the panels responsible for noise radiation [1].

Passive damping systems are generally made of viscoelastic constrained layer patches. This kind of system efficiently dissipates the vibratory energy through the viscoelastic layer shearing deformation. In order to design smart (lightweight, inexpensive, durable, robust and efficient) passive-damping systems, there is a need for reliable Finite Element Models (FEM) capable of predicting the frequency responses of structures containing viscoelastic materi-

als. Moreover, computer-aided design phases tend to be shorter and shorter. Consequently, low cost model generation and fast solution times are required in order to assess quickly at the design stage many possible technical solutions.

To achieve these objectives one must create tools to easily and accurately represent viscoelastic constitutive laws, generate multi-layer models, and, last but not least, estimate frequency responses and complex modes for tens of thousands of design points defined by frequency, temperature, layer configuration and pre-stress.

Section 2 addresses constitutive law representation and handling. Section 3 details the multi-element strategy retained to easily generate multi-layer models. Section 4 summarizes Ritz bases used to create approximate solutions fast enough to tackle the computational challenge of a design run. Precisions and performance issues associated with these solvers are also discussed.

In section 5, these analysis tools are finally used to validate various damping treatment designs for an automotive floor panel modeled using MSC/NASTRAN [2] elements and SDT [3] based solvers. The study analyzes the influence of important design variables : material selection, operating temperature, layer thickness, and treatment position.

## 2 Representing viscoelastic materials

The basic assumption of linear viscoelasticity is the existence of a relaxation function  $h(t)$  such that the stress is obtained as a convolution with the strain history. Using the Laplace transform, one obtains an equivalent representation where the material is now characterized by the *Complex Modulus*  $E$  (transform of the relaxation function)

$$\sigma(s) = E(s, T, \sigma_0)\varepsilon(s) = (E' + iE'')\varepsilon(s) \quad (1)$$

For all practical purposes, one can thus, in the frequency domain, deal with viscoelasticity as a special case of elasticity where the material properties are complex and depend on frequency, temperature, pre-stress and other environmental factors.

In practice, the complex modulus is determined experimentally using dynamic excitation [4, 5, 6]. For a given set of material test results, analysis requires knowledge of  $E(s)$  for arbitrary values of  $s$  or at least of the frequency on the Fourier axis ( $s = i\omega$ ). Three approaches must be supported in practice:

- $E(i\omega)$  is interpolated from tabulated material test data with appropriate treatments for low and high frequency asymptotes.
- $E(s)$  is represented by a rational fraction

$$E(s) = E_0 \frac{1 + \alpha_1 s + \dots + \alpha^{nn} s^{nn}}{1 + \beta_1 s + \dots + \beta^{nd} s^{nd}} \quad (2)$$

This form is of particular interest since the associated eigenvalue solvers exist (see section 4.2).

- $E(s)$  is represented using another analytical representation, in particular fractional derivatives [7].

When proper care is taken, all three approaches are capable of closely approximating material test data. They thus have the same “physical” validity. The differences are really seen in how each representation can be integrated in FEM solvers and in the validity of extrapolations outside the tested material behaviour range. On the later point, the actual process used to obtain the parameters has a strong influence, it may thus be easier to obtain a good model with a particular representation even if that representation is not inherently better.

Dependence on environmental factors (temperature, pre-stress, ...) should *a priori* be arbitrary. In

practice however, one generally assumes, and generally verifies, that environmental factors only act as shifts on the frequency [4]. Tests thus seek to characterize a master curve  $E_m(s)$  and a shift function  $\alpha(T, \sigma_0)$  describing the modulus as

$$E(s, T, \sigma_0) = E_m(\alpha(T, \sigma_0)s) \quad (3)$$

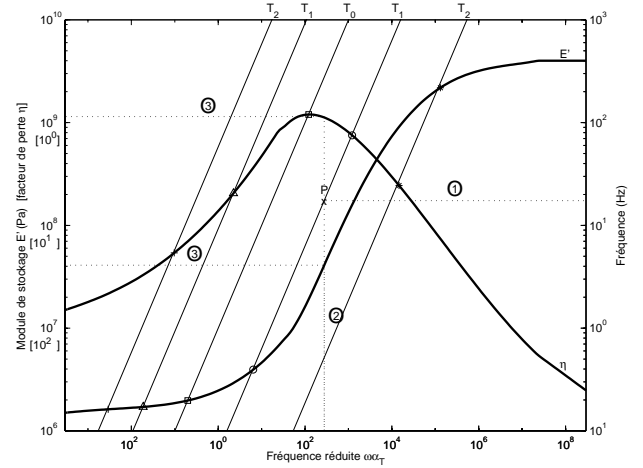


Figure 1: Reduced frequency nomogram

Classically, viscoelastic materials are thus described using a reduced frequency nomogram as shown in figure 1. For simulations, a function generating  $E$  for all values of  $s, T, \sigma_0$  must be created. This function must handle continuations outside of the range of the experimental nomogram, since these are likely to happen in a design study. Useful complements are the ability to generate nomograms, to combine experimental material characterizations into a nomogram, or to estimate the parameters of an analytic representation of test points.

## 3 Sandwich models

Viscoelastic treatments typically work in free and constrained modes [4]. In the free mode, extension of the viscoelastic layer is induced by the offset of this layer from a shell neutral plane. In the constrained mode, the difference in the extension of two stiff layers induces high shear levels in a thin viscoelastic layer.

Two main strategies have been considered to model sandwich structures : building higher order shell models [8] or connecting multiple elements. The main problem with the higher order element approach

is that developing good shell elements is very difficult so that most developments for sandwiches will not perform as well as state of the art shell elements.

The multiple element strategy is easiest to implement and has been considered here. To account properly for shear effects in the viscoelastic layer, the offsets between the neutral fiber and the shell surface must be considered. Rather than defining offsets for shell elements [9], rigid links between the shell nodes and the volume element are used here as shown in figure 2. Although this generates additional nodes (4 node layers for a single constrained layer model), this strategy accommodates all possible layer configurations. During resolution, the model is smaller since all viscoelastic volume nodes are constrained.

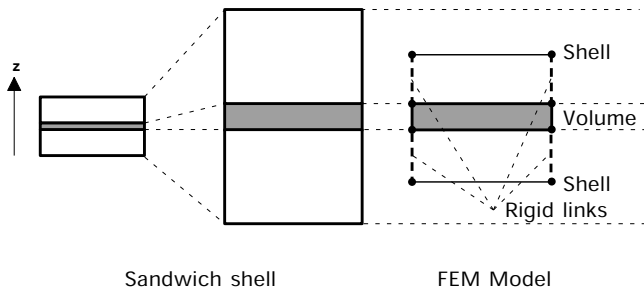


Figure 2: Shell/volume/shell model for sandwiches

For stiff layers, shells are preferred over volumes because volume element formulations are sensitive to shear locking when considering high aspect ratio (dimensions of the element large compared to thickness).

For soft layers, the use of a volume element both necessary, because shell elements will typically not correctly represent high shear through the thickness, and acceptable, because almost all their energy is associated with shear so that they will not lock in bending [10]. Note finally that shear corrections used in some FEM codes to allow bending representation with volumes must be turned off to obtain appropriate results.

Automated layer mesh generation from a selected area of a nominal shell model is a basic need for the considered study. Figure 3 shows how the strategy retained by default is to preserve the viscoelastic layer thickness through the normal to the element rather than through the node normal which is used to generate the rigid connections with stiff layers modeled with shells.

The case also clearly illustrates the non uniqueness of the choices made here. A proper study of the domain of validity of various multiple element repre-

sentations still needs to be made. This validity will in particular depend on layer thickness and material property ratios.

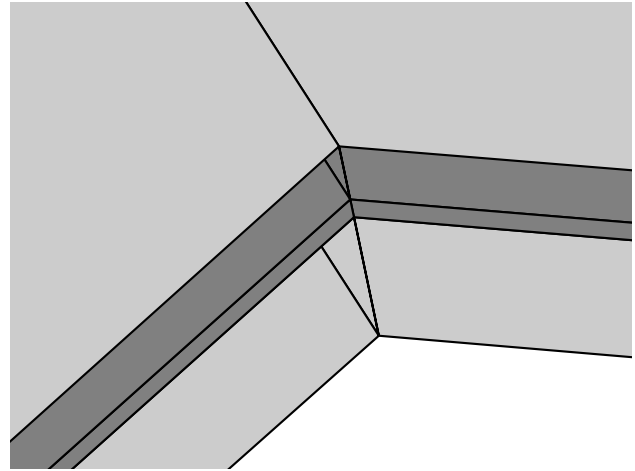


Figure 3: Layer generation for a shell

For press formed sandwiches, there are further unknowns in how the forming process affects the core thickness and material properties. In particular, most materials used for their high damping properties are also very sensitive to static pre-stress. To the authors' knowledge no significant work has been done on characterizing the actual effect of the forming process on the final properties of a curved sandwich.

A final difficulty is to deal properly with boundary conditions of the skin layers. Since differential motion of the skins plays a major role in the effectiveness of the core, the boundary conditions of each layer has to be considered separately. This is easily illustrated by the generation of cuts in constraining layers [11, 9].

## 4 Numerical solvers

Typical solvers for direct frequency response and eigenvalue solution are often quite slow and not appropriate when a range of frequencies, temperatures and designs are to be considered. The principles of the methods used for this study are summarized in this section.

### 4.1 Frequency response

The frequency response of a FEM model is obtained by solving the frequency domain dynamic equilibrium equation

$$[Z(E_i, s)]\{q\} = \{F(s)\} \quad (4)$$

at various operating points (values of frequency  $s$ , temperature  $T$  and/or pre-stress  $\sigma_0$ ). While most FEM codes will handle one instance of problem (4) easily, typical design studies require computation of a few thousand frequency points at tens of design points thus making direct frequency resolution totally impractical.

Given a constitutive law described by parameters  $E_i(s, T, \sigma_0)$ , one can use the fact that element stiffness matrices depend linearly on those parameters to build a representation of the dynamic stiffness a linear combination of constant matrices

$$Z = \left[ Ms^2 + K_e + \sum_i E_i(s, T, \sigma_0) \frac{K_{vi}(E_0)}{E_0} \right] \quad (5)$$

The ability to manipulate this expression efficiently for arbitrary material representations and both full and reduced models is the first critical step for efficient frequency response computations.

The next step is to avoid direct resolution (4) since the factorization of  $Z$  is expensive. For a given  $Z$ , iterative solvers already outperform direct ones [12].

But one can make further use of the fact that one solves many similar problems. Ref. [13] discusses the adaptation to multiple shifted problems of restarted GMRES and similar algorithms which are used classically for the iterative resolution of linear systems of equations. PSA developed a Component Mode Synthesis strategy that gives good results [14] but is not suited for design phases over a relatively wide frequency range. Automated substructuring strategies, such as described in [15], might be extended to damped cases. For section 5, one will use the approach described in Ref. [16] and summarized below.

Since one solves a class of problems, one can consider pre-conditioners that are too expensive for standard iterative methods. The tangent elastic stiffness

$$K_0 = \text{Re}(Z(E_i, 0)) \quad (6)$$

is a good candidate with the significant advantage of being real and thus faster to invert.

Spending time to get a good starting guess also makes sense since it will be used many times. As proposed in [17], a basis composed of normal modes associated with  $K_0$  and a correction for the viscoelastic loads generated by these shapes. For the subspace

$$T = \left[ \phi_{1:NM}(K_0) \quad K_0^{-1} \text{Im}(Z(\omega_0, E_{i0})) \phi_j \right], \quad (7)$$

one estimates the response using a simple model reduction

$$\{\hat{q}\} \approx [T] \left[ T^T Z(\omega_j, T, \sigma_0) T \right]^{-1} \left[ T^T \right] \{F(s)\}, \quad (8)$$

and computes the energy error associated with this approximation by evaluating the displacement residual

$$R_d = [K_0]^{-1} [Z(\omega_j, T, \sigma_0) \hat{q} - F(s)] \quad (9)$$

If this residual is large, it can be used to enrich subspace  $T$  until convergence to the exact solution is obtained [16]. Note that similar residual iterations can be used for complex eigenvalue computations [18] and that this technique can be seen as a subspace version of a conjugate gradient solver using  $K_0$  as a preconditioner [19].

## 4.2 Eigenvalue extraction

Poles and modes are non-zero solutions of the generalized eigenvalue problem

$$[Z(E_i, \lambda_j)] \{\psi_j\} = \{0\} \quad (10)$$

Given a material representation, one can distinguish two main strategies to solving (10): algebraic and non-linear solvers.

For algebraic solvers, one considers cases where the  $E_i$  have a rational fraction expression. This approach is also feasible for particular fractional derivative models [7]. An arbitrary rational fraction (2) that is proper and has distinct poles, can be represented as a sum of first order rational fractions

$$E(s) = E_\infty - \left( \sum_{j=1}^n \frac{E_j}{s + \omega_j} \right) \quad (11)$$

By introducing an intermediate field  $q_{vj} = -\frac{E_j}{(s + \omega_j)} q$ , one can rewrite (5) as a higher order first order problem, which for a single  $q_{vj}$  takes the form

$$\left[ \begin{array}{ccc|c} \left[ \begin{array}{ccc} M & 0 & 0 \\ 0 & M & 0 \\ 0 & 0 & M \end{array} \right] s + & & & \\ & 0 & -M & 0 \\ \left[ \begin{array}{ccc} K_e + E_\infty K_v & 0 & K_v \\ E_j M & 0 & \omega_j M \end{array} \right] & \left\{ \begin{array}{c} q \\ sq \\ q_v \end{array} \right\} & = & \left\{ \begin{array}{c} 0 \\ F \\ 0 \end{array} \right\} \end{array} \right] \quad (12)$$

Depending on the operators available in the FEM code, one may want to use a second order form. The *Anelastic Displacement field* method [20] thus writes the model as

$$\left[ s^2 \left[ \begin{array}{cc} M & 0 \\ 0 & 0 \end{array} \right] + s \left[ \begin{array}{cc} 0 & 0 \\ 0 & \frac{K_v}{E_j} \end{array} \right] + \left[ \begin{array}{cc} K_e - E_\infty K_v & K_v \\ K_v & \frac{\omega_j}{E_j} K_v \end{array} \right] \right] \left\{ \begin{array}{c} q \\ q_{vj} \end{array} \right\} = \left\{ \begin{array}{c} F \\ 0 \end{array} \right\} \quad (13)$$

with possibly multiple  $q_{vj}$  for each pole in (11).

But this form has no mass associated with  $q_{vi}$  which may be a problem for some solvers. An alternative is the GHM method [21], which represents  $E$  in the form

$$E(s) = E_{\infty} \left( 1 + \sum_{j=1}^n \frac{\alpha_j}{s^2 + 2\zeta_j \omega_j s + \omega_j^2} \right) \quad (14)$$

and defines fields  $q_{vj} = \frac{\alpha_j}{s^2 + 2\zeta_j \omega_j s + \omega_j^2} q$ . Note however that not all rational functions can be represented in form (14).

While transformation to a standard constant matrix form allows the use of eigenvalue solvers present in FEM codes, the increase in the number of degrees of freedom can be significant and the high connectivity between elements of the sandwich means that the sparsity pattern of the considered matrices is rather full. Strategies for improved solvers that are not too sensitive to the order augmentation are discussed in Ref. [18].

Non-linear eigenvalue solvers, search a direct resolution of (10). A full search of the complex plane being impractical for large models, such solvers take into account the expected pattern of solutions. Since the considered damping is still relatively low, one can have meaningful estimates of the complex modes by defining a reference eigenvalue problem where the stiffness is constant.

From this initial estimate, continuation techniques [22] or estimation using specific transfer functions [17] can be used to converge to the true solution. The later solution is the only one applicable for interpolated tabular material data which is only known on the Fourier axis ( $s = i\omega$ ) and was used to generate pole estimates in section 5.

### 4.3 Solver performance

Two types of solvers need to be considered. Solvers for design need to be very fast and somewhat accurate. Solvers for verification need to be very reliable and not too slow. Design solvers considered here use a fixed basis such as (7) and optimize the resolution of (8). Solutions where residual (9) is computed and one iterates until convergence are typically much slower and will be called *verification solvers*.

Table 1 gives an indication of CPU times for basic steps of the considered solvers for floor panel considered in section 5. MSC/NASTRAN version 70.7 [2] and SDT 5.0 [3] are compared on an SGI Origin 2000

parallel computer. While as expected NASTRAN runs faster, the speedup is not by orders of magnitude (in other cases it is smaller [9]). The Matlab/SDT environment is thus very appropriate for the selected objectives of introducing design solvers and testing verification ones.

Assembly times correspond to the building of element matrices and combination to form real mass and stiffness matrices. Reassembly times correspond to the computation of (5). In reduced solutions, computing  $T^T Z T$  is quite long. It is thus preferable to use a reduced version of (5) where each constant matrix is reduced separately. This approach is however not feasible for verification solvers which need to compute a residue. Thus the projection step puts a critical limitation on the ability to optimize verification solvers.

Table 1: CPU times in seconds on a SGI Origin 2000 of some key steps (design A+B of section 5 with 58766 DOFs, N.A. : not applicable)

	NAST.	SDT
$M - K$ Assembly	45	N.A.
Factorization of K	20	67
F/B substitution (7 vect)	1.85	4.02
75 normal modes	166	730
Z reassembly	N.A.	6
Projection $T^T Z T$	N.A.	25
Factorization of Z	77	153
F/B substitution (1 vect)	2.7	4.1

The typical solution considered in section 5 is a parametric study with variations of frequency and one or two other parameters (temperature, layer thickness, ...). A design will thus typically consider at least 1000 frequency points and 10 parametric points. Even with NASTRAN's efficient solution in 80 s (not counting reassembly), such a run would take more than 9 days and thus be quite unacceptable for design. By comparison, all operations needed to build basis (12) (with 152 vectors) are performed in 445 s and a 10 240 design point study runs in 612 s (a speedup of 1300). For iterative verification solvers, performance is quite sensitive to the basis size and increase drastically when large bases need to be enriched regularly. Tools to eliminate vectors from a given basis are thus still needed.

At the nominal design point, design solvers are typically quite accurate as illustrated in figure 4. For very different operating conditions, this may however

not always be true for large deviations as illustrated in figure 10.

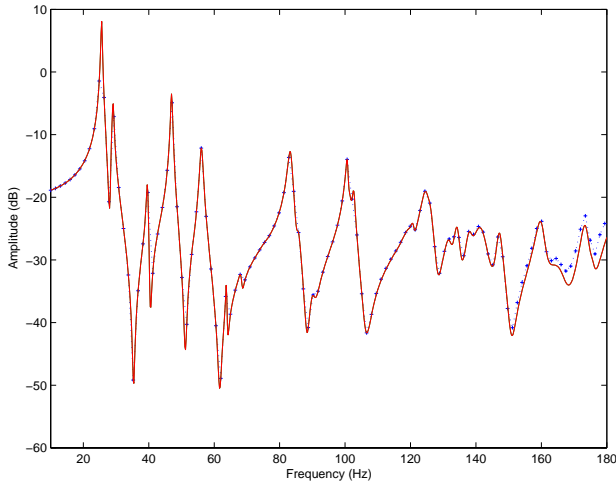


Figure 4: Exact and approximate FRFs for the floor panel of section 5 (Case B1/Ta)

## 5 Applications to a floor panel

Parameters particularly relevant for the design of damping treatments include

- material properties for a given temperature/frequency range
- layer thickness
- treatment shape and location.

Understanding how these parameters affect the effectiveness of the damping treatment is the main difficulty for optimization as will be illustrated in this section.

### 5.1 Model

The proposed tools will be illustrated for the case of an automotive floor panel shown in figure 5. The nominal model was meshed by PSA and read in Universal File Format. After addition of the damping treatment models (creation of node layers described in section 3), an elastic eigenvalue computation was run in MSC/NASTRAN [2] whose element matrices were imported back into the SDT [3] to run various computations shown here.

The panel is clamped on its edge and two point loads, shown in figure 5, are considered for FRF computations. The nominal model contains 7998 nodes and 7813 elements. A single free layer adds 2195

nodes and 1908 elements. But the model order remains the same since all nodes of the free layer are slave. A constrained layer model adds three node layers (6595 nodes) and two element layers (3816 elements). The model size increases by  $6 \times 2195 = 13170$  DOFs.

The initial model used eight viscoelastic damping treatment areas shown in gray. Two additional patches, indicated by arrows were also considered in configurations not show here.

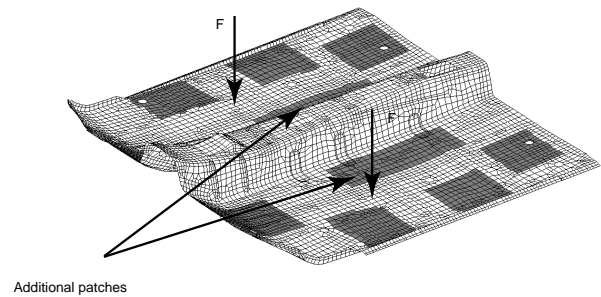


Figure 5: FE model of an automotive floor panel

The following designs were considered:

- A1 : a free layer treatment (working in extension) covering the nominal patches with a nominal 0.67 mm steel layer and a 2.47 mm viscoelastic layer;
- B1 : a constrained layer treatment with a nominal 0.67 mm steel layer, a  $50 \mu\text{m}$  viscoelastic layer and a 0.3 mm steel constraining layer;

### 5.2 Material selection

When selecting a material to be used in a viscoelastic damping treatment, it is essential to understand how the material behaves in the temperature/frequency range of interest. Before actually defining a geometry, one can display reduced frequency bands on the master modulus curve. For example, figure 6 illustrates that material SM50e has low stiffness and loss factor for low frequency (10-200 Hz) near room temperature operation. The same material would be efficient for sub-zero temperatures or a higher frequency band (5-20 kHz).

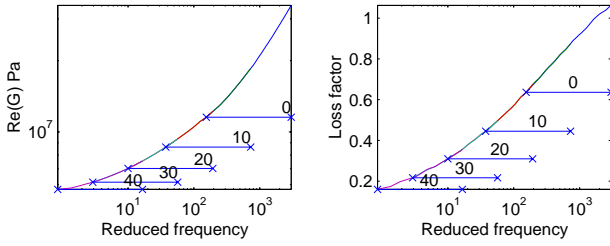


Figure 6: Nomogram of a viscoelastic material SM50e with frequency bands associated to the 10-200 Hz range at various temperatures.

Figure 7 illustrates the same dependence for a much stiffer material that will be considered for unconstrained layer designs in section 5.4. Now the operating range of interest is above loss factor peak, so that reducing temperature will actually decrease damping. The smaller band overlap also illustrates a higher sensitivity to operating conditions.

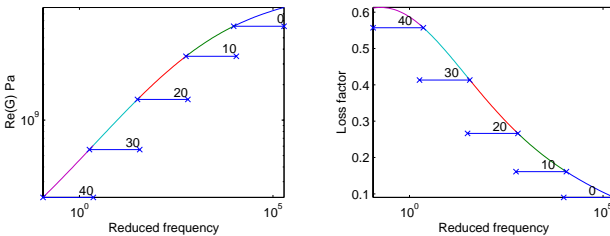


Figure 7: Nomogram of a viscoelastic material PL3023 with frequency bands associated to the 10-200 Hz range at various temperatures.

Once a particular design is selected, it is important to validate its robustness to temperature variations. This can be done by computing FRFs for a frequency/temperature range as shown in figure 8. While an improvement can be noticed around 20°C the damping here is quite low and the plot is thus difficult to interpret.

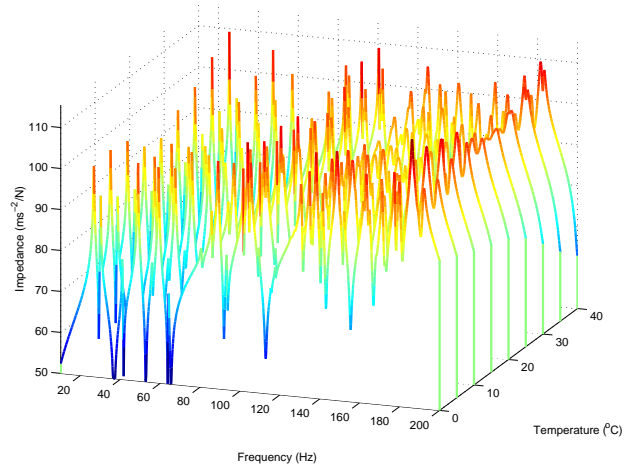


Figure 8: FRFs for a frequency/temperature range (Case B1/Ta).

Pole tracking as shown in figure 9 is a useful alternative. For the considered case it confirms that indeed optimal damping is achieved near 20°C.

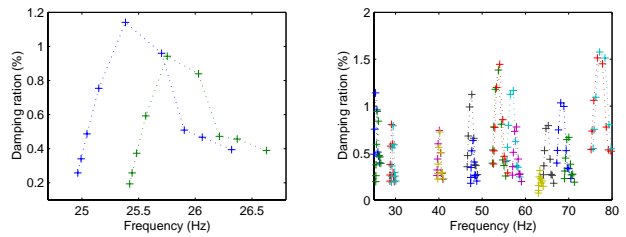


Figure 9: Pole tracking on the 0+40°C range (Case B1/Ta)

Care must however be taken in using fixed basis reduced models over a wide parametric range. Figure 10 for example shows the classical temperature optimum but also a strong increase of damping at very low temperatures. This effect disappears when changing the tangent elastic stiffness (6) to reflect a much higher nominal value of the viscoelastic layer. Indicators to warn of likely result inaccuracy are thus needed as intermediates between design and verification solvers.

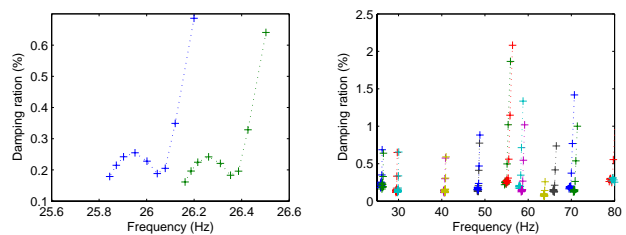


Figure 10: Pole tracking on the -40+40°C range (Case B1/SM50e)

### 5.3 Thickness optimization

An exact study of the influence of thickness variations is an enormous task since it implies remeshing of the layers and full solution of the frequency response and/or modes. To get a first cut at the task, one can linearize the influence of thickness on the element matrices.

For a constrained viscoelastic configuration, the constrained layer essentially works in shear. Shear stiffness being inversely proportional to thickness, one can approximate the stiffness contribution of a constrained layer of another thickness by

$$K_{vi}(h_v, E_i) \approx \frac{h_{v0}}{h_v} \frac{E_i(s, T, \sigma_0)}{E_0} K_{vi}(E_0) \quad (15)$$

Similarly, for relatively low constraining layer thickness, the energy is essentially associated to the layer extension and thus proportional to thickness. One thus has, for an elastic constraining layer

$$K_{ci}(h_c) \approx \frac{h_c}{h_{c0}} K_{ci}(E_i) \quad (16)$$

Based on these approximations, one can compute the evolution of poles and FRFs with thickness. Figure 11 shows the evolution of the damping of 4 poles as a function of layer thickness for patch configuration B1, material TA at 20°C (nominal viscoelastic layer at  $h_{v0} = 50\mu m$  and constraining at  $h_{c0} = .3mm$ ). This map indicates that dissipation could be augmented by increasing  $h_c$  to .5 or .7mm. For  $h_v$  the 50 $\mu m$  nominal seems reasonable but the optimum differs for each pole (and the reliability of estimates at higher frequencies can be questioned).

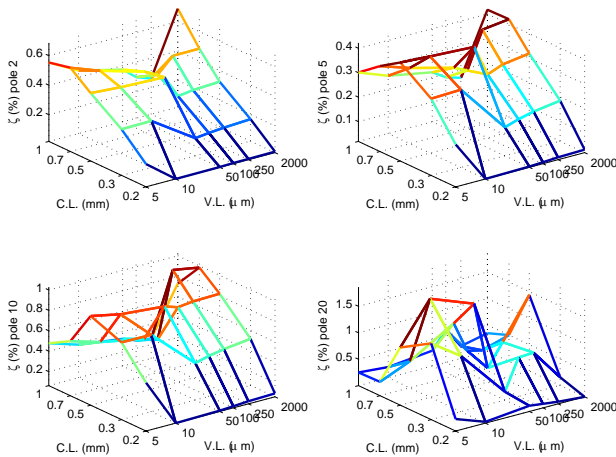


Figure 11: Influence of layer thickness on the damping ratio of pole 1.

Figure 12 shows that a direct exploitation of the responses computed for this range of layer thickness

is difficult. The retained objective function is thus the RMS response of the acceleration transfer functions over the 10-200 Hz range which is of interest.

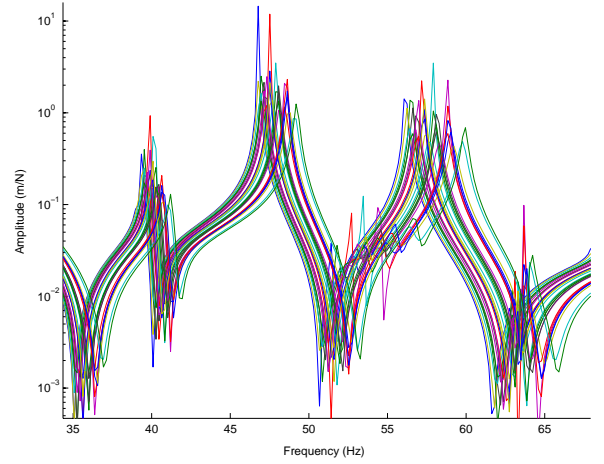


Figure 12: FRFs for a range of layer thickness.

The map of RMS responses in figure 13 confirms the need to increase the constraining layer thickness (to .5mm). For the viscoelastic layer thickness the variations are quite low which confirms the pole tracking indications.

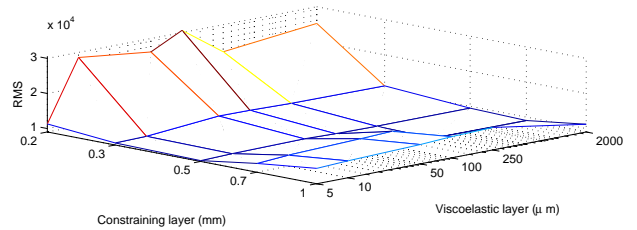


Figure 13: Influence of layer thickness on the RMS acceleration for range 10-200 Hz.

### 5.4 Treatment nature

This section compares three designs (free layer A1, constrained layer B1 with TA and SM viscoelastic materials). Figure 14 shows the difficulty of comparing designs from FRF plots. While third octave bands give easier interpretation, the temperature axis is missing. Temperature effects are shown in figure 15 where one sees that design B1-Ta is actually as good as design A1 at room temperature while the mass added by the treatment is 50% less.

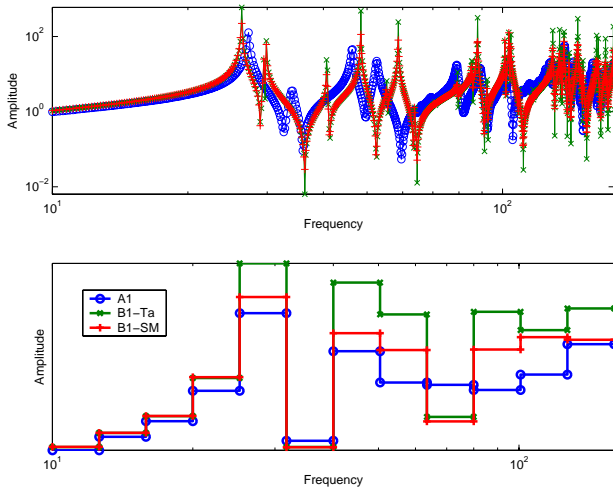


Figure 14: RMS responses for various designs. FRF and third octave averages.

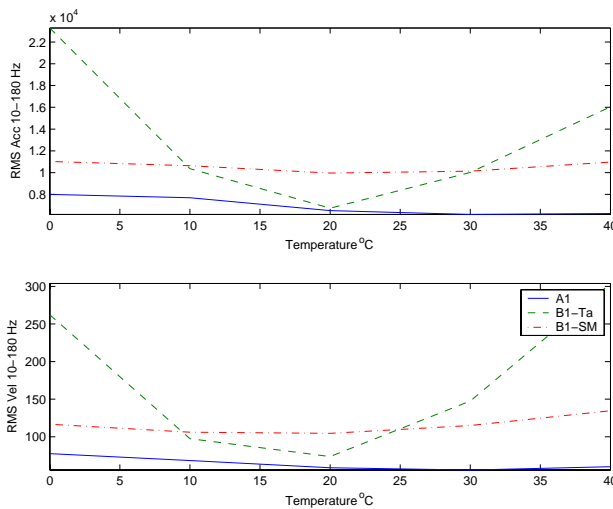


Figure 15: RMS responses for various designs.

## 6 Conclusion

This paper illustrated an ongoing effort to develop effective design tools to select damping treatments. While enormous progress has been made in the ability to handle models of sizes interesting for design, many questions remain to be answered.

For mesh generation, a tool was created to generate single and multiple layer models of shells and thin volumes connected by rigid links to represent the actual position of the bond between layers. But systematic studies of the validity of shell/volume/shell models and of possible evolutions of material properties during sandwich forming process are still needed.

For design solvers, fixed basis reduced approximations are the only ones likely to allow coverage of

a large design space. The actual range of accuracy of such solutions is however difficult to establish, so that low cost indicators warning of probable solution inaccuracy are clearly needed. For verification solvers, optimizing combinations of substructuring and iterative tools will provide much needed improvement to the methods currently available.

Finally, the availability of these tools will enhance the ability to select among many possible technical choices. Developing standardized procedures help this process is another area needing a major efforts.

## References

- [1] **Stawicki, S., Bohineust, X. and Dupuy, F.**, *Dimensionnement des traitements amortissants de structures automobiles par application du calcul éléments finis en dynamique*, SIA Article 93011, 1993.
- [2] **MSC/NASTRAN**, Quick Reference Guide 70.7, MacNeal Shwendler Corp., Los Angeles, CA, February, 1998.
- [3] **Balmès, E. and Leclère, J.**, Structural Dynamics Toolbox 5.0 (for use with MATLAB), SD-Tools, Paris, France, <http://www.sdtools.com>, July 2002.
- [4] **Nashif, A., Jones, D. and Henderson, J.**, *Vibration Damping*, John Wiley and Sons, 1985.
- [5] **Allen, B. R.**, *A Direct Complex Stiffness Test System for Viscoelastic Material Properties*, Proceedings of Smart Structures and Materials, February 1996.
- [6] **Kergourlay, G. and Balmès, E.**, *Conception d'un banc de mesure des propriétés de films viscoélastiques*, IME2002, Besançon, Juillet 2002.
- [7] **Bagley, L. and Torvik, P.**, *Fractional calculus - A different approach to the analysis of viscoelastically damped structures*, AIAA Journal, Vol. 21, No. 5, pp. 741-748, 1983.
- [8] **Kant, T. and K., S.**, *Free vibration of isotropic, orthotropic and multilayer plates based on higher order refined theories*, Journal of Sound and Vibration, Vol. 241, No. 2, pp. 319-327, 2001.

- [9] **Balmès, E.** and **Bobillot, A.**, *Analysis and Design Tools for Structures Damped by Viscoelastic Materials*, IMAC, February 2002.
- [10] **Plouin, A.** and **Balmès, E.**, *A test validated model of plates with constrained viscoelastic materials*, IMAC, pp. 194–200, 1999.
- [11] **Mead, D.** and **Markus, S.**, *The Forced Vibration of a Three Layer, Damped Sandwich Beam with Arbitrary Boundary Conditions*, Journal of Sound and Vibration, Vol. 10, No. 2, pp. 163–175, 1969.
- [12] **Sauvage, O., Aubry, D., Jezequel, L., X., O.** and **C., S.**, *Modélisation de l'amortissement non-standard et des vibrations d'éléments d'un groupe moto-propulseur en moyennes fréquences*, Cinquième Colloque National En Calcul de Structure, Giens, pp. 205–212, 2001.
- [13] **Feriani, A., Perotti, F.** and **Simoncini, V.**, *Iterative system solvers for the frequency analysis of linear mechanical systems*, Computer Methods in Applied Mech. and Eng., Vol. 13-14, pp. 1719–1739, 2000.
- [14] **Germès, S.** and **Van Herpe, F.**, *Model reduction and substructuring for computing responses of structures containing frequency-dependent viscoelastic materials*, SPIE's 9th Annual International Symposium on Smart Structures and Materials, March 2002.
- [15] **Bennighof, J., Kaplan, M., Muller, M.** and **Kim, M.**, *Meeting the NVH Computational Challenge: Automated Multi-Level Substructuring*, IMAC, pp. 909–915, 2000.
- [16] **Kergourlay, G., Balmès, E.** and **Clouteau, D.**, *Interface model reduction for efficient FEM/BEM coupling*, ISMA, Leuven, September 2000.
- [17] **Plouin, A.** and **Balmès, E.**, *Steel/viscoelastic/steel sandwich shells. Computational methods and experimental validations.*, IMAC, pp. 384–390, 2000.
- [18] **Bobillot, A.** and **Balmès, E.**, *Iterative techniques for eigenvalue solutions of damped structures coupled with fluids*, Submitted to SDM Conference, 2002.
- [19] **Alvin, K. F.**, *Efficient Computation of Eigenvector Sensitivities for Structural Dynamics*, AIAA Journal, Vol. 35, No. 11, pp. 1760–1766, November 1997.
- [20] **Lesieutre, G.** and **Bianchini, E.**, *Time Domain Modeling of Linear Viscoelasticity Using Augmenting Thermodynamic Fields*, SDM Conference, AIAA paper 93-1550-CP, pp. 2101–2109, 1993.
- [21] **Golla, D.** and **Hughes, P.**, *Dynamics of viscoelastic structures – A time domain finite element formulation*, Journal of Applied Mechanics, Vol. 52, pp. 897–906, 1985.
- [22] **Daya, E.** and **Potier-Ferry, M.**, *A numerical method for non linear eigenvalue problems. Application to vibration of viscoelastic structures*, Computers and Structures, Vol. 79, pp. 533:541, 2001.